Preprint
UCRL-JC-144454

Tissue Imaging for Cancer Detection Using NIR Autofluorescence

S.G. Demos, M. Staggs, R. Gandour-Edwards, R. Ramsamooj, R. de Vere White

This article was submitted to
Society of Photo-Optical Instrumentation Engineers 47th Annual Meeting, Seattle, WA, July 6-11, 2002

February 11, 2002

Tissue imaging for cancer detection using NIR autofluorescence

Stavros G. Demos[*a], Mike Staggs[a],
Regina Gandour-Edwards[b], Rajen Ramsamooj[b], Ralph deVere White[b]

[a]Lawrence Livermore National Laboratory, PO Box 808, L-411, Livermore, CA 94551.

[b]UC Davis Cancer Center, 4501 X Street, Sacramento, CA 95817

ABSTRACT

Near infrared imaging using elastic light scattering and tissue fluorescence under long-wavelength laser excitation are explored for cancer detection. Various types of normal and malignant human tissue samples were utilized in this investigation. A set of images of each tissue sample is recorded. These images are then compared with the histopathology of the tissue sample to reveal the optical fingerprint characteristics suitable for cancer detection. The experimental results indicate that the above approaches can help image and differentiate cancer from normal tissue.

Key words: Tissue Imaging, Backscattering, Polarization, Tissue autofluorescence

1. INTRODUCTION

Optical spectroscopy has been widely used to acquire fundamental knowledge about physical, chemical, and biological processes that occur in biomaterials. Various research groups have attempted to classify and diagnose tissue states using fluorescence and Raman spectroscopy [1-4]. The main fluorophores in tissues exhibit maximum absorption at photon energies higher than 2 eV. As a result, most tissue spectroscopy research has employed UV to visible light sources from 250-nm to 600-nm. The main active fluorophores in this spectral region are tryptophan, collagen, elastin, NAD(P)H, flavins and prophyrins. The disadvantage of these wavelengths is their short photon penetration depth in tissues, which leads to extraction of information only from superficial tissue layers.

Raman scattering measurements in tissues show the presence of a long Stokes spectral wing that makes the observation of the fine details in the Raman scattering vibrational spectrum difficult. The intensity of the Stokes spectral wing becomes weaker as the pump wavelength increases. This spectral wing has been considered as noise and is usually subtracted from the Raman spectral profile using complex fitting parameters to acquire the spectral features associated with the Raman active vibrational modes. It was only recently shown that the origin of this background signal in the far-red and near infrared (NIR) spectral region in Raman scattering measurements of tissues is due to emission by photoexcited fluorophores [5]. It was also shown in the same paper that the NIR autofluorescence intensity from cancer and normal human breast tissue is very different suggesting a new way to detect breast cancer.

The objective of our effort is to employ hyperspectral imaging techniques to investigate the ability of polarized light scattering in combination with native tissue fluorescence under long-wavelength laser excitation to image tissue components with special attention for the case of cancer detection. Our experimental approach involves imaging of various types of malignant with contiguous non-neoplastic human tissue samples using cross-polarized elastic light scattering at 700-nm, 850-nm and 1000-nm and tissue autofluorescence in the 700-1000-nm spectral region under 532-nm and 632.8-nm laser excitation.

2. EXPERIMENTAL ARRANGEMENT

The human tissue specimens studied in this work were obtained from fresh surgical resections. The experiments precede fixation for pathologic assessment without compromise of histologic quality. In order to simplify the procedure required for the execution of optical spectroscopy experiments on human samples, we have built a compact spectroscopic imaging system that was positioned in a lab space adjacent to surgical pathology at the UC Davis Medical Center. Figure 1 shows the schematic layout of the key optical components composing this prototype instrument. The experimental setup involves polarizers (P) and appropriate optical filters (F) while low power lasers and a white light source are used as the illumination sources. The images of the sample are acquired using a camera lens coupled to a liquid nitrogen cooled CCD detector. A polarizer and appropriate filters are positioned in front of the camera lens to select the polarization state and spectral band for the image formation. For the autofluorescence

* Correspondence: Email: demos1@llnl.gov; Telephone: (925) 423 3388; Fax: (925) 423 2463

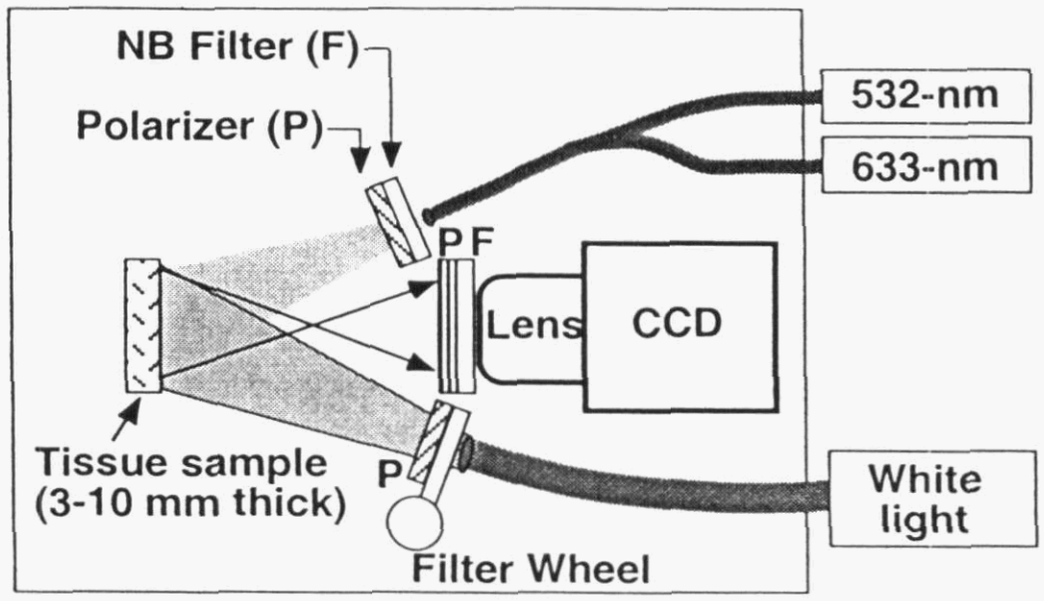

Figure 1: Schematic layout of the key optical components of the instrumentation to perform *in-vitro* measurements of human tissue samples immediately after surgery. The experimental setup involves polarizers (P) and appropriate optical filters (F). Two lasers and a white light source coupled with optical fibers are used to illuminate the sample.

imaging experiments, the photoexcitation is provided by a 632.8-nm He-Ne laser and by a 532-nm diode-pumped Nd:YAG laser. The laser light is transferred into the imaging compartment of the system using optical fibers. The diverging output beam from the fiber is used to provide nearly uniform illumination of the sample. A polarizer and a narrow band interference filter were positioned in front of the output of the fiber to ensure monochromatic illumination and linearly polarized illumination. For the light scattering imaging experiments, a white light source coupled to a fiber bundle is used to provide a nearly uniform illumination of the sample. A polarizer is positioned at the output of this fiber with its polarization orientation perpendicular to that of the polarizer located in front of the camera lens in order to record only the perpendicular polarization image component and thus, remove the specular reflection component from the image. Illumination of the sample with 700-nm, 850-nm, and 1000-nm is achieved using 40-nm bandwidth interference filters at the aforementioned wavelengths positioned on a filter wheel located in front of the fiber bundle. With this imaging system, a set of 7 images is recorded for each sample. More specifically, we record the cross-polarized light scattering images under 700-nm, 850-nm and 1000-nm illumination, the NIR (700-nm to 1000-nm) autofluorescence images under 532-nm and 632.8-nm photoexcitation and the two orthogonal polarization components of tissue autofluorescence under 632.8-nm excitation. These images are subsequently compared with the histopathology map of this same tissue specimen obtained using conventional methods (hematoxylin-eosin stain).

3. EXPERIMENTAL RESULTS

Specimens obtained from more that 60 patients have been studied to date. In the rest of this document, we will show and discuss typical examples of our experimental results. The aim is to demonstrate the potential of each approach to provide imaging of tissue components including the detection of cancer.

Figure 2 shows a ≈ 4-cm X 3-cm human breast tissue sample with multifocal high grade ductal carcinoma in-situ surrounded by fibrous stroma, with an adjacent area of fatty infiltration. Fig. 2a shows the cross-polarized light scattering image of the sample under 700-nm illumination. Figs. 2b and 2c show the fluorescence images in the 700 to 1000-nm spectral region under 532-nm and 632.8-nm laser excitation, respectively. Fig. 2d shows the degree of polarization image of the NIR emission under 632.8-nm excitation. From the images of the sample shown in fig. 2, only the NIR fluorescence image under 632.8-nm excitation (fig. 2c) shows a correlation with the histopathological assessment map of the sample. The 1-mm diameter areas of higher emission coincide with the location of the ductal carcinoma lesions in the sample. The integrated NIR emission intensity arising from these cancerous parts of the sample is higher by a factor of ≈1.5 when compared to that of the normal tissue.

Figure 3 shows as set of images obtained from a liver specimen. A histologic section of this specimen show a well circumscribed 0.8 x 0.5 cm nodule. The histologic features of the nodule are those of a hepatoblastoma. Fig. 3a shows the cross-polarized light scattering image under 700-nm illumination. Figs. 3b and 3c show the NIR autofluorescence images under 532-nm and 632.8-nm laser excitation, respectively. The cancer nodule is visible in all images shown in figure 3 as a brighter in intensity feature. More specifically, in figure 3a (cross-polarized light scattering image under 700-nm illumination) the digitized intensity in the area of the cancer nodule is higher by a factor of ≈0.13 when compared to that of the adjacent normal liver tissue. This intensity difference between the two tissue components is further increased in the NIR autofluorescence images and it becomes ≈ 0.4 and ≈ 0.65 under 532-nm and 632.8- nm excitation, respectively. This difference in image intensity allows for best visualization of the cancer nodule especially in the NIR autofluorescence images (figs. 3b and 3c).

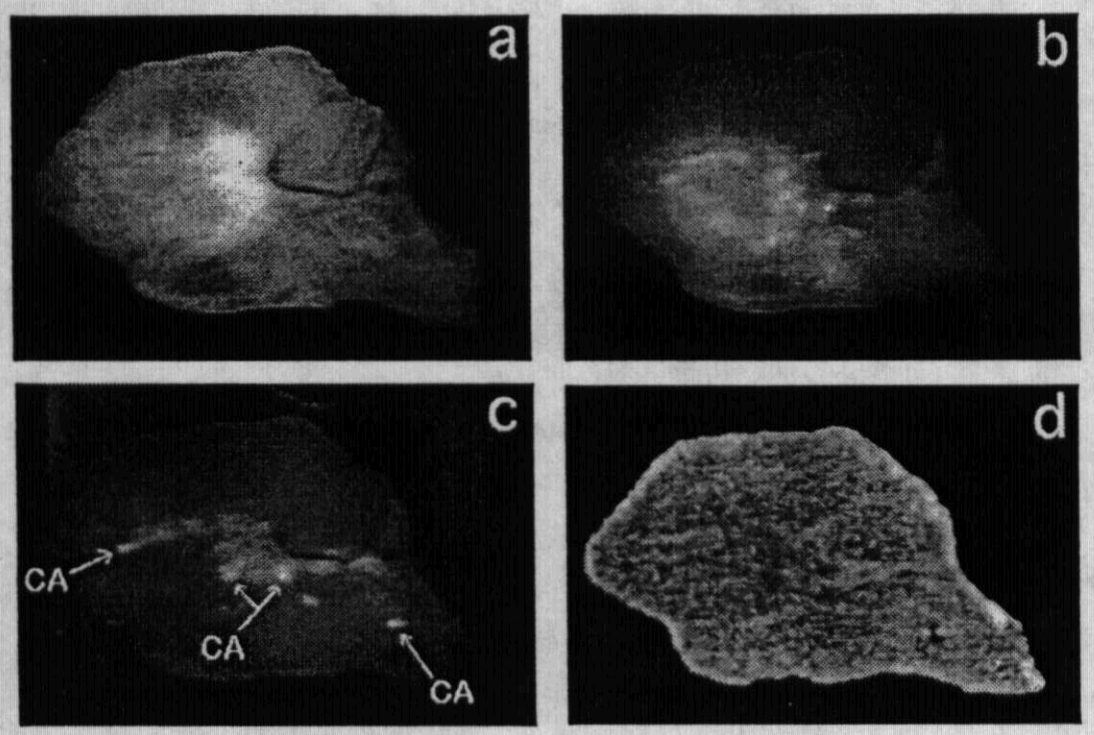

Figure 2:. Images of a human breast tissue sample with multifocal high-grade ductal carcinoma in-situ. a) cross-polarized light scattering image at 700-nm. NIR fluorescence images under b) 532-nm and c) 632.8-nm laser excitation. d) degree of polarization image of tissue autofluorescence under 632.8-nm excitation. CA: cancer

Figure 4 shows images of a kidney specimen containing a cancerous lesion. Figs. 4a shows the cross-polarized light scattering image under 700-nm illumination. Fig. 4b shows the NIR fluorescence images under 632.8-nm laser excitation. Fig. 4c is the image obtained from a division of the NIR autofluorescence digitized image under 532-nm excitation over that recorded under 632.8-nm excitation. The histologic sections of this kidney specimen shows that there is a poorly demarcated nodule measuring 1.0-cm x 0.6-cm with histologic features that suggest renal cell carcinoma. This nodule is surrounded by normal kidney. At one side of the tissue (top) is normal fat tissue that surrounds the kidney. In the optical images, the cancer lesion appears as a brighter in intensity feature in the light scattering images and as darker feature in the NIR autofluorescence images when compared to the normal kidney. This is demonstrated in the images shown in figs. 4a and 4b. In the light scattering image under 700-nm illumination (fig. 4a), the digitized intensity of the area of the cancer nodule is higher by a factor of ≈0.7 when compared to that of the adjacent normal kidney tissue. On the other hand, the autofluorescecne intensity under 632.8-nm excitation arising from the cancerous parts of the specimen exhibits lower intensities by a factor of ≈0.4 when compared to that of the normal kidney tissue. The fat lesion located on the upper side of this specimen (as imaged) is better visualized in the ratio image shown in fig. 4c where the fat tissue is clearly differentiated from the kidney tissue. In the latter image, the normal kidney cannot be differentiated from the cancer lesion.

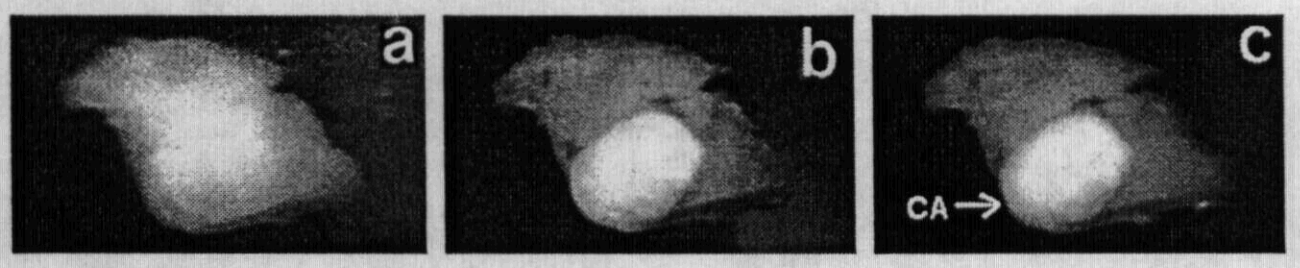

Figure 3:. Images of a human liver tissue sample with hepatoblastoma. a) Cross-polarized light scattering image at 700-nm. NIR fluorescence images under b) 532-nm and c) 632.8-nm excitation. CA: cancer.

4. DISCUSSION

There are two different concepts under investigation. The first concept examines polarized light scattering spectral imaging. The second concept involves imaging of various tissue types using the NIR emitted light under 632.8-nm and 532-nm excitation. The experimental results provided in this document are representative of our results to date. The results shown on figure 1 are consistent with results previously reported on breast tissue. The imaging approach we have utilized, rather than a point by point measurement utilized before, allows for better evaluation of the limit detection. The NIR fluorescence image shown in fig. 2c demonstrates that this method can be used to detect small cancer lesions (1-mm or smaller) in a field of normal tissue.

The images attained using elastic light scattering delineate differences in absorption and scattering between tissue components. On the other hand, porphyrins may be the principal tissue chromophores contributing to NIR autofluorescence under red excitation. The enhancement of porphyrin production in tumors has been investigated as a method to produce endogeneously synthesized photosensitizers for PDT [6]. Increased porphyrin content in the

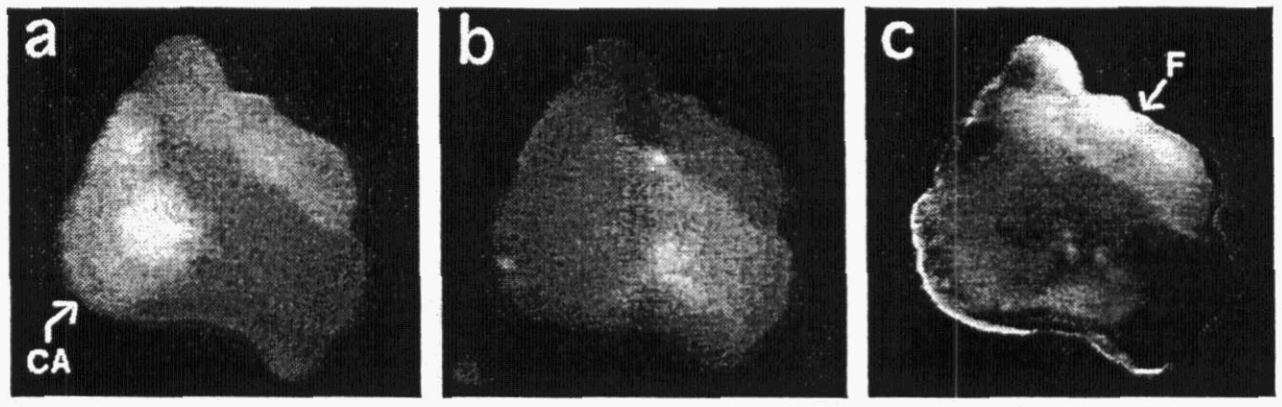

Figure 4:. Images of a human kidney tissue with renal cell carcinoma. a) Cross-polarized image at 700-nm. b) NIR fluorescence images under 632.8-nm laser excitation. c) Ratio of NIR autofluorescence image under 532-nm excitation over that under 632-nm excitation. CA: cancer, N: Normal, F: Fat

tumors in humans and experimental animals, mainly hepatomas, has been reported [7-8]. It has also been reported that the porphyrin content in tumors is not always higher than the contiguous non-neoplastic tissues and depends on the type of cancer and host tissue [9]. Assuming that the autofluorescence signal arises mainly from porphyrins, our experimental observations are consistent with the aforementioned reports.

The experimental results shown in figs. 3 and 4 indicate that the light scattering properties of the tissue component may influence but not dictate the measured intensity of the NIR autofluorescence signal. The scattering signal from the tumor in liver and in kidney is higher than that of the normal tissue. However, the NIR autofluorescence from the tumor in kidney is lower than that of the normal tissue while the opposite is the case in liver. This indicates the novel properties of NIR autofluorescece imaging method. This capability is further enhanced by utilizing excitation at different wavelengths. The 1-mm tumor lesions in the breast specimen are visible in the NIR autofluorescence images under 632.8-nm excitation but not under 532-nm excitation. It must be noted that we have not been able to extract any additional information using the degree of polarization of the NIR autofluorescece.

The NIR autofluorescence imaging method may offer a way to monitor and/or image the porphyrin content in tissues. There is strong evidence that the heme-biosynthetic pathway, and therefore the production of porphyrins, is disturbed in neoplastic disease. This may be the reason that the NIR autofluorescence images offer high contrast between normal and tumor tissue. An imaging system that is based on this method could provide assistance to a surgeon to visualize the tumor margins for more accurate and complete removal of cancerous tissue. It may also be useful as a diagnostic tool for an *in-vivo*, real-time pathological assessment to complement light microscopy performed on fixed tissue sections, the current "gold standard" for the histo-pathologic diagnosis of human diseases.

ACKNOWLEDGMENTS

This work was performed in part at Lawrence Livermore National Laboratory under the auspices of the U.S. Department of Energy under Contract W-7405-Eng-48 through the Institute for Laser Science and Applications. This research is supported by the California Cancer Research Program.

REFERENCES

1. Alfano R. R., Tata B., Cordero J., Tomashefsky P., Longo F. W., and Alfano M. A., Laser induced fluorescence spectroscopy from native cancerous and normal tissues, IEEE J. Quantum Electron., **QE-20**, 1507-1511 (1984)
2. Kortum R. R., Rava R. P., Petras R. E., Fitzmaurice M., Sivak M. and Feld M. S., Spectroscopic diagnosis of colonic dysphasia, Photochem & Photobio. **53**(6) 777-786, (1991)
3. Schomacker K.T., Frisoli J.K., Compton C.C., Flotte T.J., Richter J.M., Nishioka N.S., Deutsch T.F., "ultraviolet laser-induced fluorescence of colonic tissue - basic biology and diagnostic potential", Lasers in Surgery And Medicine **12**, 63-78 1992
4. J. D. Pitts, R. D. Sloboda, K. H. Dragnev, E. Dmitrovsky, M. A. Mycek, "Autofluorescence characteristics of immortalized and carcinogen-transformed human bronchial epithelial cells", J. Biom. Opt., **6**, 31, 2001
5. Zhang G., Demos S. G., and Alfano R.R., "Far-red and NIR spectral wing emission from tissues under 532-nm and 632-nm photo-excitation", Lasers in the Life Sciences, **9**, 1-16 (1999)
6. Z. Malik, H. Lugaci, Destruction of erythroleukemic cells by photoactivation of endogenous porhyrins, Br. J. Cancer, 156, 589 (1987).
7. M. Udagawa, Y. Horie, C. Hirayama, "Aberrant porphyrin metabolism in Hepatocellular carcinoma", Biochem. Med., **31**, 131 (1984).
8. N. M. Navone A. L. Frisardi, E. R. Resnik, A. M. del C. Batlle, C. Polo, "Porphyrin biosynthesis in human breast cancer", Med. Sci. Res., **16**, 61 (1968).
9. B. Zawirska, Comperative porphyrin content in tumors with contiguous non-neoplastic tissues, Neoplasma, **26**, 223 (1979).